IEEE ICCC 2023 1570907048

Channel Estimation for Extremely Large-Scale Massive MIMO Systems in Hybrid-Field Channel

Xingxing Peng[1], Lei Zhao[1], Yuan Jiang[1,*], Jingjing Liu[1] and Weidan Li[2]
[1]School of Electronics and Communication Engineering, Sun Yat-Sen University, Shenzhen 518107, China.
[2]GuangDong Communications and Networks Institute, Guangzhou 510000, China.
*Corresponding author
Emails: pengxx26@mail2.sysu.edu.cn, zhaolei27@mail.sysu.edu.cn, jiangyuan3@mail.sysu.edu.cn,
liujj77@mail.sysu.edu.cn, liwd@gdcni.cn

2023 IEEE/CIC International Conference on Communications in China (ICCC) | 979-8-3503-4538-4/23/$31.00 ©2023 IEEE | DOI: 10.1109/ICCC57788.2023.10233609

***Abstract*—Extremely large-scale massive multiple-input multiple-output (XL-MIMO) is the key technique for future 6G communications. However, the extremely large aperture arrays make the accurate channel state information (CSI) acquisition more difficult. To solve this problem, we focus on the location information (i.e., the angle and range) of the scatters in the far-field and near-field areas, and propose a hybrid-field channel estimation algorithm for the XL-MIMO system. Specifically, firstly by simplifying the hybrid-field channel model, we transform the channel estimation problem into the position parameters estimation problem for the far-field and near-field scatters. Then, we propose a hybrid-field channel estimation algorithm based on the estimation of the angle and range of the different scatters. Finally, numerical results show the superior performances of the proposed algorithm in comparison to the existing methods.**

***Index Terms*—Extremely large-scale massive MIMO, channel estimation, hybrid-field channel, parameter estimation.**

I. Introduction

As the key enabler for the intelligent information society by 2030, 6G networks are anticipated to perform better than 5G, in terms of peak data rate, spectrum efficiency, and energy efficiency [1]. More sophisticated and effective technologies must be investigated and utilized to achieve these breakthrough performances. One of them is the extremely large-scale massive multiple-input multiple-output (XL-MIMO) technology. The XL-MIMO technology is the further evolution and upgrading of massive multiple-input multiple-output (MIMO) technology, where the base station (BS) deploys a huge number of antennas to achieve improved spectrum efficiency and energy efficiency [2].

To fully exploit the potential gain provided by the XL-MIMO, the BS must provide accurate channel state information (CSI) during downlink signal preprocessing [3]. However, the demand for precise CSI in the XL-MIMO system poses a severe challenge to traditional channel estimation. Firstly, the increasing number of antennas adds the dimension of the channel matrix, which might be difficult to estimate. Secondly, as pilot overhead increases, traditional linear channel estimation methods, such as least squares (LS) and minimum mean square error (MMSE) methods are no longer applicable [4]. Thirdly, the characteristics of the hybrid-field channel, i.e., near-field propagation [5] and spatial non-stationarity [2], make channel estimation more challenging.

The main channel estimation methods are those based on the compressive sensing (CS) theory and channel parameter estimation for the XL-MIMO system. The channel estimation problem can be transformed into a sparse matrix reconstruction problem. Thus, Some CS algorithms, such as orthogonal matching pursuit (OMP) [6], [7], can be used to estimate the sparse channel. Typically, the authors in [7] have applied this method to a sparse angle-domain channel estimation. Moreover, it has been demonstrated that there are different scatters may be in different regions for the XL-MIMO system in [8], which has proposed sparse channel estimation algorithm with estimating the far-field and near-field path components, respectively. To enhance the estimation accuracy, the sparse Bayesian learning (SBL) approach is another solution to the sparse signal recovery problem. For example, in [9], a mixed channel estimation algorithm via the joint support estimation and SBL-based framework was proposed. In [10], an efficient SBL-based channel estimation scheme was utilized to satisfy the computational efficiency.

Avoiding dealing with the channel matrix directly, the methods of channel parameter estimation also can effectively improve the channel estimation performance. The paper [11] investigated the estimation of each parameter of the channel based on the Space-Alternating Generalized Expectation-Maximization (SAGE) algorithm, which jointly estimates the angle of arrival (AoA) and the range of the near-field scatters. To achieve high channel estimation accuracy especially in the case of low signal-to-noise ratio (SNR), a two-stages SAGE-based channel estimation algorithm was proposed in [12]. What's more, for higher resolutions and lower computational complexity, these methods were also used including estimation of signal parameters via rotational invariance technique (ESPRIT) [13], and multiple signal classification (MUSIC) algorithms [14], [15], which separately estimate the AoA and the range from the scatter to the BS. The paper [16] proposed obtaining the location parameters of the far-field and near-field sources by isolating the different types of sources while avoiding the eigendecomposition. Traditionally, the spherical

This work was supported in part by the Key-Area Research and Development Program of Guangdong Province under Grant 2019B090904014, in part by the National Natural Science Foundation of China under Grant 62101608.

wavefronts are well approximated by planes, the corresponding physical model being regarded as the plane wave model (PWM). However, in the massive MIMO scenarios, the wavefront of an incident wave emitted from the scatter exhibits spherical curvature, and more complex but more accurate models such as the spherical wave model (SWM) might be required [17]. Further, the paper [18] introduced a parabolic wave model (ParWM), which is more accurate than the PWM but less complex than the spherical wave model (SWM). Compared with the channel estimation based on the PWM, the channel estimation based on the ParWM needs estimate not only the AoA but also the range between the scatter and the BS, and it also saves the complexity of radical calculation for the SWM.

The XL-MIMO channel can be more accurately modeled considering the hybrid-field communication environment, where both the far-field and near-field scatters exist [8]. Based on the location parameters estimation of the far-field and near-field scatters, in this paper, a channel estimation method for the XL-MIMO system is proposed to improve the estimation accuracy. Specifically, simplifying the XL-MIMO hybrid-field channel model in [8] by approximating spheres with paraboloids, we transform the channel estimation problem into the position parameters estimation problem for the different scatters. Further, we propose a channel estimation algorithm to obtain the separate position parameters of the far-field (i.e., the AoA) and near-field scatters (i.e., the AoA and range). What's more, we distinguish the far-field and near-field scatters by the comparison of the power spectrum. Particularly, when the hybrid-field channel exists a kind of scatters only, the algorithm can also identify the far-field or near-field scatters. Simulation results show that the proposed algorithm can achieve higher accuracy than the existing algorithms.

The rest of the paper is organized as follows. In Section II, we respectively describe the near-field and far-field channel and simplify the hybrid-field channel model. In Section III, we firstly introduce the rank-reduced MUSIC algorithm which is used to estimate the AoA and the range of the scatters, and then propose the hybrid-field channel estimation algorithm. Simulation results and conclusion are provided in Section IV and Section V, respectively.

Notation: Lower-case and upper-case boldface letters $\mathbf{a}$ and $\mathbf{A}$ denote a vector and a matrix, respectively. $\mathbf{a}^H$ and $\mathbf{A}^H$ denote the conjugate transpose of vector $\mathbf{a}$ and matrix $\mathbf{A}$, respectively.

II. SYSTEM MODEL

For the extremely large-scale massive MIMO system, as shown in Fig. 1, we consider that the BS is composed of $M = 2N + 1$ antennas, and the distance between adjacent antennas is d. The signals transmitted by users may arrive at the BS along the line-of-sight (LoS) path or be reflected by the scatters. Without loss of generality, we consider the last-jump scatters of the paths. The user antenna is regarded as the scatter for the LoS path.

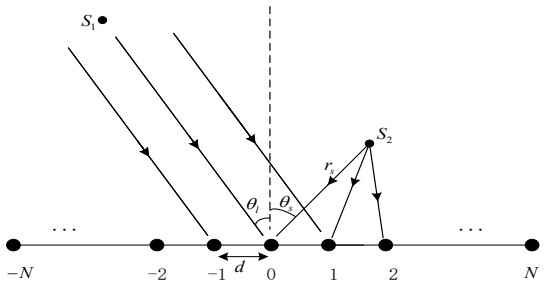

Fig. 1. The array model for the hybrid field

Considering the practical XL-MIMO system, there are both the far-field scatters (Fig. 1, S_1) and the near-field scatters (Fig. 1, S_2). The widely adopted boundary between the far-field and near-field regions is the Rayleigh distance $Z = \frac{2D^2}{\lambda}$, where D and λ represent the array aperture and the wavelength, respectively [5]. That is, when the distance from the scatter to the BS is larger than Z, the scatter is located in the far field, otherwise the scatter belongs to the near-field scatter. In this section, we will firstly introduce the channel consisting of the far-field and near-field path components respectively, and then simplify the hybrid-field channel model.

A. Far-Field Channel

The far-field channel model is established based on the plane wave assumption. Thus, there is one parameter for the far-field path component, that is, the AoA. The phase difference of the n-th array element relative to the central array element can be represented by

$$\Delta\tau_{n,l} = \frac{2\pi d}{\lambda} n \sin\theta_l, \tag{1}$$

where $\theta_l \in \left[-\frac{\pi}{2}, \frac{\pi}{2}\right]$ denotes the AoA of the l-th far-field path.

Furthermore, the far-field steering vector $\mathbf{a}(\theta_l) \in C^{(2N+1)\times 1}$ can be represented by

$$\begin{aligned}\mathbf{a}(\theta_l) = [&e^{-j\frac{2\pi d}{\lambda}N\sin\theta_l}, \ldots, e^{-j\frac{2\pi d}{\lambda}\sin\theta_l}, \\ &1, e^{j\frac{2\pi d}{\lambda}\sin\theta_l}, \ldots, e^{j\frac{2\pi d}{\lambda}N\sin\theta_l}].\end{aligned} \tag{2}$$

Therefore, the far-field channel $\mathbf{h}_{\mathrm{far}}$ can be expressed as

$$\mathbf{h}_{\mathrm{far}} = \sum_{l=1}^{L} g_l \mathbf{a}(\theta_l) \in C^{(2N+1)\times 1}, \tag{3}$$

where L is the number of the far-field scatters, and g_l represents the amplitude for the l-th path.

B. Near-Field Channel

By approximating spheres with paraboloids, the near-field channel is modeled based on the parabolic wave assumption in a low-complexity way. The model includes two parameters, the AoA $\theta_s \in \left[-\frac{\pi}{2}, \frac{\pi}{2}\right]$ and the range $r_s < \frac{2D^2}{\lambda}$ between the s-th near-field scatter and the central array element.

The phase difference of the n-th array element relative to the central array element can be represented by

$$\Delta\tau_{n,s} = \frac{2\pi}{\lambda}\left(r_{n,s} - r_s\right), \tag{4}$$

where $r_{n,s} = \sqrt{r_s^2 + (nd)^2 - 2ndr_s \cos\left(\frac{\pi}{2} - \theta_s\right)}$ represents the distance from the s-th near-field scatter to the n-th antenna.

According to the Fresnel approximation, $\Delta\tau_{n,s}$ can be simplified as

$$\Delta\tau_{n,s} \approx \omega_s n + \phi_s n^2, \tag{5}$$

where $\omega_s = -\frac{2\pi d}{\lambda}\sin(\theta_s)$, $\phi_s = \frac{\pi d^2}{\lambda r_s}\cos^2(\theta_s)$.

The near-field steering vector $\mathbf{b}(\theta_s, r_s) \in C^{(2N+1)\times 1}$ can be represented by [19]

$$\begin{aligned}\mathbf{b}(\theta_s, r_s) = [&e^{j\left(-\omega_s N + \phi_s(-N)^2\right)}, \ldots, e^{j(-\omega_s+\phi_s)},\\ &1, e^{j(\omega_s+\phi_s)}, \ldots, e^{j\left(\omega_s N + \phi_s N^2\right)}].\end{aligned} \tag{6}$$

Therefore, the near-field channel $\mathbf{h}_{\text{near}}$ can be expressed as

$$\mathbf{h}_{\text{near}} = \sum_{s=1}^{S} g_s \mathbf{b}(\theta_s, r_s) \in C^{(2N+1)\times 1}, \tag{7}$$

where S and g_s denote the number of the near-field scatters and the amplitude of the s-th near-field path, respectively.

C. Hybrid-field channel

For the XL-MIMO system, some scatters are far away from the BS, while some are relatively close to the BS. Therefore, the hybrid-field channel model can be represented by

$$\mathbf{h} = \sum_{l=1}^{L} g_l \mathbf{a}(\theta_l) + \sum_{s=1}^{S} g_s \mathbf{b}(\theta_s, r_s), \tag{8}$$

where the first and the second item represent the far-field and near-field path components, respectively. $\mathbf{a}(\theta_l)$ depends on the AoA of the l-th far-field scatter, while $\mathbf{b}(\theta_s, r_s)$ is directly associated with the AoA and the range of the s-th near-field scatter. By simplifying the hybrid-field model, we can transfer the channel estimation problem into the position parameters estimation problem for the different scatters.

We can see that the phase difference (1) under the far-field condition can be regarded as a special case in (5) for $r_s \to \infty$. Thus, $\mathbf{a}(\theta_l)$ can be represented by $\mathbf{b}(\theta_l, \infty)$.

Moreover, the pilot received by the BS is denoted by $\mathbf{y} = \sqrt{P}\mathbf{h} + \mathbf{w}$, where P is the transmitted power and $\mathbf{w} \in C^{(2N+1)\times 1}$ is the additive Gaussian noise with zero means and unit variance.

III. PROPOSED ALGORITHM

A. The Rank-Reduced MUSIC Algorithm

For the array signal processing, the observation space of signal can be divided into a signal subspace and a noise subspace, which are orthogonal to each other [14]. Under the hybrid-field conditions, the properties of the signal subspace and noise subspace still exist. The MUSIC algorithm decomposes the covariance matrix of the received signal, and the obtained eigenvectors associated with the large eigenvalues form the signal subspace, while the remains constitute the noise subspace. By utilizing the orthogonality between the two subspaces, the MUSIC algorithm can estimate the AoA and the range of scatters. The space spectrum function can be constructed as

$$f_{\text{MUSIC}} = \frac{1}{\mathbf{b}^H(\theta, r)\mathbf{U}_n\mathbf{U}_n^H\mathbf{b}(\theta, r)}, \tag{9}$$

where $\mathbf{U}_n$ represents the noise subspace, $\mathbf{b}(\theta, r)$ is the array steering vector, θ and r are the AoA and the range of the scatter. Under the far-field condition, r can be taken as $+\infty$.

To reduce the complexity of the estimation algorithm, we choose to estimate the AoA and the range of the scatter separately. Due to the symmetry of the array, the steering vector (6) can be decomposed as follows [14]

$$\begin{aligned}\mathbf{b}(\theta, r) &= \boldsymbol{\xi}(\theta)\boldsymbol{\eta}(\theta, r)\\ &= \underbrace{\begin{bmatrix} e^{j(-N)\omega} & & & & \\ & e^{j(-N+1)\omega} & & & \\ & & \ddots & & \\ & & & 1 & \\ & & & \iddots & \\ & & e^{j(N-1)\omega} & & \\ e^{jN\omega} & & & & \end{bmatrix}}_{\boldsymbol{\xi}(\theta)} \underbrace{\begin{bmatrix} e^{j(-N)^2\phi} \\ e^{j(-N+1)^2\phi} \\ \vdots \\ e^{j(-1)^2\phi} \\ 1 \end{bmatrix}}_{\boldsymbol{\eta}(\theta, r)}\end{aligned} \tag{10}$$

where $\boldsymbol{\xi}(\theta) \in C^{(2N+1)\times(N+1)}$ contains the AoA of the scatter, and $\boldsymbol{\eta}(\theta, r) \in C^{(N+1)\times 1}$ includes the AoA and the range of the scatter. Substitute (10) into (9), we get

$$\begin{aligned}f_{\text{MUSIC}} &= \frac{1}{\boldsymbol{\eta}^H(\theta, r)\boldsymbol{\xi}^H(\theta)\mathbf{U}_n\mathbf{U}_n^H\boldsymbol{\xi}(\theta)\boldsymbol{\eta}(\theta, r)}\\ &= \frac{1}{\boldsymbol{\eta}^H(\theta, r)\boldsymbol{\Lambda}(\theta)\boldsymbol{\eta}(\theta, r)},\end{aligned} \tag{11}$$

where $\boldsymbol{\Lambda}(\theta) = \boldsymbol{\xi}^H(\theta)\boldsymbol{U}_n\boldsymbol{U}_n^H\boldsymbol{\xi}(\theta) \in C^{(N+1)\times(N+1)}$, which contains the AoA and is a non-negative definite conjugate symmetric matrix. Because of $\boldsymbol{\eta}(\theta, r) \neq 0$, the sufficient and necessary condition for $\boldsymbol{\eta}^H(\theta, r)\boldsymbol{\Lambda}(\theta)\boldsymbol{\eta}(\theta, r) = 0$ is that $\boldsymbol{\Lambda}(\theta)$ is a singular matrix. With the number of scatters less than N, the column rank of the noise subspace $\mathbf{U}_n$ must be larger than or equal to $N+1$. That is, $\boldsymbol{\Lambda}(\theta)$ is a full-rank matrix. When the AoA is searched for the actual direction of arrival, $\boldsymbol{\Lambda}(\theta)$ is reduced to a singular matrix. Through the MUSIC algorithm, the AoA can be represented by

$$\hat{\theta} = \arg\max_{\theta} \frac{1}{\det[\boldsymbol{\Lambda}(\theta)]}, \tag{12}$$

where operators $\arg\max(\cdot)$ and $\det(\cdot)$ represent the maximum value and the determinant, respectively.

B. Proposed Hybrid-field Channel Estimation

In the hybrid-field scenario, the position information of the far-field scatters is determined by the AoA θ_l, and for the near-field scatters it depends on both the AoA θ_s and the range r_s between the scatter and the BS. Therefore, it is critical to distinguish the different scatters efficiently. The method to estimate the hybrid-field channel called hybrid-field rank-reduced MUSIC (H-RM) is proposed in this paper based on

the position parameters estimation of the scatters. The basic idea is that, firstly, estimating the AoAs of all the scatters by the spectral peak search. Secondly, distinguishing the far-field and near-field scatters, which includes two steps. The first step aims to differentiate between the far-field and near-field scatters initially, while the second step needs to further isolate the near-field one from the far-field scatters which has the same AoA. Thirdly, the range is estimated for the near-field scatter. And finally, the path amplitudes need to be obtained. The specific algorithm is shown in **Algorithm 1**.

Algorithm 1 Proposed H-RM algorithm

Input: $\mathbf{y}$, P, γ

1: **Initialization**: $\Omega_{\mathrm{f}} = \Omega_{\mathrm{n}} = \emptyset$
2: Obtain K estimated AoAs $\hat{\theta}_k$ via (12)
3: **for** $k = 1, 2, \cdots, K$ **do**
4: Compute $f(\hat{\theta}_k, \infty)$ via (13)
5: **if** $f(\hat{\theta}_k, \infty) > \gamma$ **then**
6: $\Omega_{\mathrm{f}} = \Omega_{\mathrm{f}} \bigcup \hat{\theta}_k$
7: **else**
8: $\Omega_{\mathrm{n}} = \Omega_{\mathrm{n}} \bigcup \hat{\theta}_k$
9: **end if**
10: **end for**
11: Compute $f(\hat{\theta}_k, r), \forall \hat{\theta}_k \in \Omega_{\mathrm{f}}$ via (9)
12: **if** $f(\hat{\theta}_k, r)$ exists a wave crest **then**
13: $\Omega_{\mathrm{n}} = \Omega_{\mathrm{n}} \bigcup \hat{\theta}_k$
14: **end if**
15: Estimate the ranges of the near-field scatters via (14)
16: Estimate the amplitudes via (15)-(16)
17: Obtain the estimated hybrid-field channel $\hat{\mathbf{h}}$ via (17)

Output: $\hat{\mathbf{h}}$

The procedures of **Algorithm 1** can be explained as follows. Let Ω_{f} and Ω_{n} respectively denote the estimated AoAs sets of the far-field and near-field scatters, which are both initialized as the empty set $\emptyset$. Firstly, the algorithm obtains K estimated AoAs $\hat{\theta}_k$ for all the scatters by the search for the space spectrum function (11) and (12).

Secondly, we distinguish the near-field and far-field scatters by two steps. The first step is the coarse distinction (Lines 3 to 10), which roughly distinguishes the far-field and near-field scatters among all the estimated angles. Then, the refined distinction (Lines 11 to 14) recognizes the possible near-field scatter from the AoA set of the far-field scatters with the same AoA, which isolates the different scatters completely.

1) Coarse distinction: The Line 4 regards r as ∞ for differentiating between the far-field and near-field scatters. By substituting the estimated AoA $\hat{\theta}_k$ and $r \to \infty$ into equation (9), the space spectrum function can be expressed as

$$f\left(\hat{\theta}_k, \infty\right) = \frac{1}{\mathbf{b}^H\left(\hat{\theta}_k, \infty\right) \mathbf{U}_n \mathbf{U}_n^H \mathbf{b}\left(\hat{\theta}_k, \infty\right)}, \tag{13}$$

where $k = 1, 2, \ldots, K$.

It is known that if the scatter is in the far-field region, the result $f(\hat{\theta}_k, \infty)$ obtained from (13) should be larger than that of the near-field scatter. By comparing the results with the threshold γ[1] and updating the AoAs set Ω_{f} and Ω_{n} (Lines 5 to 9), we distinguish the far-field and near-field scatters coarsely in the hybrid field.

2) Refined distinction: It will initially be regarded as a far-field scatter if the near-field scatter shares the same AoA $\hat{\theta}_k$ as the far-field one. Therefore, it is critical to further distinguish the near-field scatters from the far-field scatters. By substituting the estimated AoA $\hat{\theta}_k \in \Omega_{\mathrm{f}}$ of the far-field scatters into (9), as shown in Line 11, a one-dimensional spectral search for the range is performed in the near-field region $\left(0, \frac{2D^2}{\lambda}\right)$.

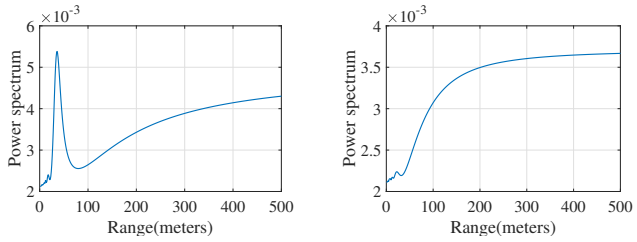

Fig. 2. The comparison of the power spectrum for the range. (a) The near-field and far-field scatter have the same AoA. (b) The near-field and far-field scatter have different AoA.

If there is a wave crest for the spectrum function $f(\hat{\theta}_k, r)$ as shown in Fig. 2(a), the angle $\hat{\theta}_k$ not only corresponds to a far-field scatter, but also to a near-field scatter. If the spectrum does not display a wave crest but rather is smoother as shown in Fig. 2(b), the angle belongs to a far-field scatter. Based on the updated AoAs set Ω_{n} (Lines 12 to 14), all the far-field and near-field scatters have been distinguished so far.

Thirdly, we can get the ranges of the near-field scatters. On the one hand, the range where the wave crest appears for the refined distinction is the range of the near-field scatter, which has the same AoA as the far-field scatter. On the other hand, the range $\hat{r}_k$ of remaining near-field scatters can also be obtained by the spectral search in the near-field region. Moreover, the range and the AoA are automatically matched to the same scatter. The range $\hat{r}_k$ of the near-field scatters based on the AoA $\hat{\theta}_k$ can be represented as

$$\hat{r}_k = \arg\max_r \frac{1}{\mathbf{b}^H(\hat{\theta}_k, r) \mathbf{U}_n \mathbf{U}_n^H \mathbf{b}(\hat{\theta}_k, r)}. \tag{14}$$

Finally, we can obtain the amplitude $\hat{g}_s$ and channel estimation $\hat{\mathbf{h}}$. That is, both the AoAs and the ranges of the scatters estimated, we can get the estimation of the amplitudes for each path by such as LS algorithm, as follows

$$[\hat{g}_1, \ldots, \hat{g}_L, \hat{g}_1, \ldots, \hat{g}_S]^T = \frac{1}{\sqrt{P}} \left(\mathbf{A}^H \cdot \mathbf{A}\right)^{-1} \cdot \mathbf{A}^H \cdot \mathbf{y}, \tag{15}$$

where L and S denote the size of the sets Ω_{f} and Ω_{n}

[1]By substituting all the angles θ within the search scope $\left[-\frac{\pi}{2}, \frac{\pi}{2}\right]$ and $r \to \infty$ into equation (9), we can see that when the angle $\hat{\theta}_k$ meets the actual AoA of the far-field scatter, the result $f(\hat{\theta}_k, \infty)$ will be larger than that of all the other angles. Therefore, it's easy to determine the threshold γ in order to identify the far-field scatter.

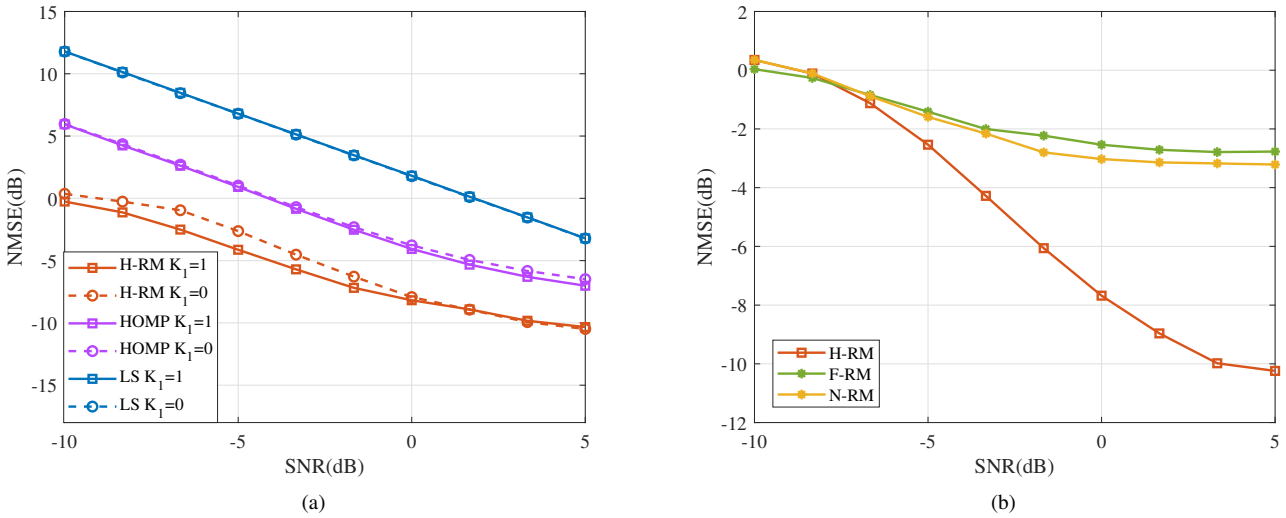

Fig. 3. The NMSE performance comparison against the SNR. (a) Comparing the proposed algorithm with the existing methods. (b) Comparing the proposed algorithm with the F-RM and N-RM methods without distinguishing different scatters.

respectively, and the matrix $\mathbf{A}$ consists of the steering vectors as follows

$$\mathbf{A} = \left[\mathbf{a}\left(\hat{\theta}_1\right), \ldots, \mathbf{a}\left(\hat{\theta}_L\right), \mathbf{b}\left(\hat{\theta}_1, \hat{r}_1\right), \ldots, \mathbf{b}\left(\hat{\theta}_S, \hat{r}_S\right)\right]. \quad (16)$$

After estimating the location information (i.e., the AoA, or the AoA and the range) of the far-field and near-field scatters, the hybrid-field channel can be expressed as

$$\hat{\mathbf{h}} = \sum_{l=1}^{L} \hat{g}_l \mathbf{a}\left(\hat{\theta}_l\right) + \sum_{s=1}^{S} \hat{g}_s \mathbf{b}\left(\hat{\theta}_s, \hat{r}_s\right). \quad (17)$$

Here, we provide the computational complexity analysis of our proposed channel estimation algorithm. The total complexity of the proposed H-RM algorithm is described as $\mathcal{O}(M^3+N_\theta(M-K)(N+1)(M+N+1)) + \mathcal{O}((M+1)(M-K)((N_r-1)K_1+K+N_rS))$, which N_θ and N_r is the number of the AoA and the range search.

IV. SIMULATION RESULTS

In this section, simulation results of the proposed method are analyzed. We consider the number of BS antennas $2N+1 = 475$. The wavelength is set as $\lambda = 0.01$ meters, and $d = \lambda/2$. We calculate the normalized mean square error (NMSE) of the estimated channel $\hat{\mathbf{h}} \in C^{(2N+1)\times 1}$ as $\mathrm{E}\left[\|\hat{\mathbf{h}}-\mathbf{h}\|^2/\|\mathbf{h}\|^2\right]$.

As shown in Fig. 3, we consider $L = 1$ far-field scatter and $S = 1$ near-field scatter in the hybrid-field channel. Fig. 3(a) compares the proposed H-RM algorithm with the existing HOMP [8] and classical LS algorithms against the SNR. It is demonstrated that whether there is or not the same AoA between the far-field and near-field scatter (i.e., $K_1 = 1$ or $K_1 = 0$), the proposed H-RM algorithm can achieve considerably lower NMSEs than the existing methods. Therefore, we can see that the H-RM algorithm gets higher resolution by estimating the AoAs of all the scatters and the ranges of the near-field scatters, and can distinguish the different scatters, especially when the near-field scatter has the same AoA as the far-field scatter. As shown in Fig. 3(b), the NMSE performance achieved by H-RM is much better than the far-field RARE MUSIC (F-RM) and near-field RARE MUSIC (N-RM), which ignore distinguishing the near-field and far-field scatters. On the one hand, the F-RM and N-RM methods only consider the far-field or near-field path components, which mismatch the practical XL-MIMO system. On the other hand, the location parameters of far-field (i.e., the AoA) and near-field scatters (i.e., the AoA and the range) are different, which cannot be regarded as the single case.

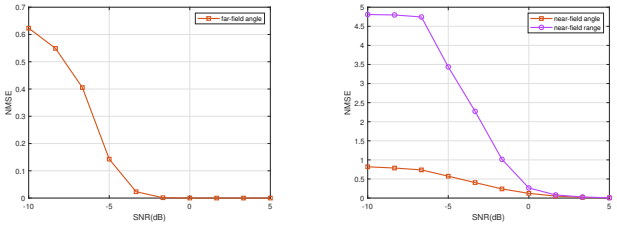

Fig. 4. The NMSE performances of the location parameters estimation against the SNR (a) for the far-field scatter and (b) for the near-field scatter.

Fig. 4 exhibits the performances of the proposed algorithm for the parameters estimation in the hybrid-field channel. For the AoA estimation of the far-field scatters, Fig. 4(a) shows that the proposed algorithm can achieve the accurate estimation, and the NMSE reduces dramatically with the SNR increasing. Fig. 4(b) depicts that for the near-field scatters, the proposed algorithm has a high accuracy of the estimation for the AoA and the range.

Fig. 5 further evaluates the effectiveness of the proposed algorithm in comparison to the existing methods, when there are only the far-field or near-field scatters in the hybrid field.

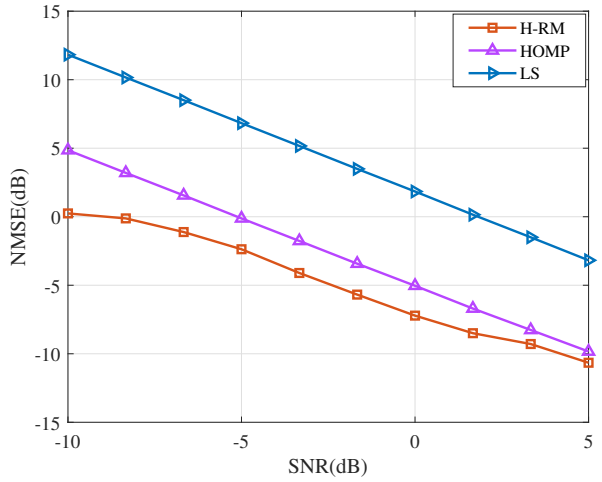

(a)

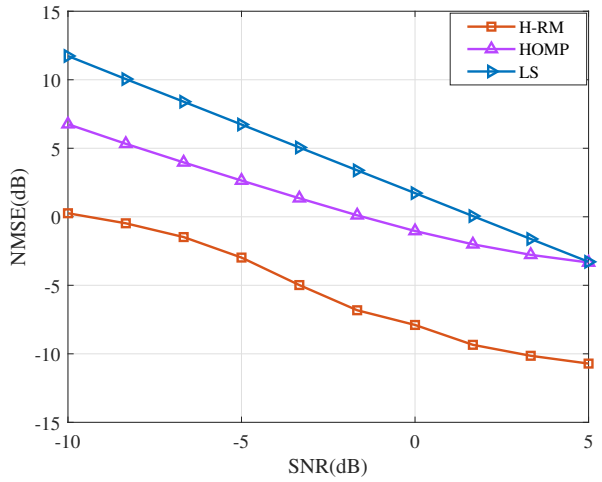

(b)

Fig. 5. The NMSE performances comparison when the channel is far-field or near-field. (a) Far-field channel with $L = 2$, $S = 0$. (b) Near-field channel with $L = 0$, $S = 2$.

By identifying the far-field or near-field scatters and estimating the corresponding position parameters, Fig. 5(a) and 5(b) show that the H-RM algorithm outperforms the HOMP and LS methods.

V. CONCLUSION

In this paper, a hybrid-field channel estimation method has been proposed to explore the XL-MIMO channel. We simplified the hybrid-field channel model which considers the far-field and near-field path components simultaneously. What's more, it was shown that the far-field path component can be regarded as the special case of the near-field path component. Furthermore, we proposed a hybrid-field channel estimation algorithm based on the estimation of the AoA and the range for the far-field and near-field scatters. The simulation results showed that the proposed method can achieve better NMSE performance than the existing methods. Moreover, it was demonstrated that distinguishing the near-field and far-field scatters can help obtain accurate channel estimation.

REFERENCES

[1] Z. Zhang, Y. Xiao, Z. Ma, M. Xiao, Z. Ding, X. Lei, G. K. Karagiannidis, and P. Fan, "6G wireless networks: Vision, requirements, architecture, and key technologies," *IEEE Veh. Technol. Mag.*, vol. 14, no. 3, pp. 28-41, Sep. 2019.

[2] E. D. Carvalho, A. Ali, A. Amiri, M. Angjelichinoski, and R. W. Heath, "Non-stationarities in extra-large-scale massive MIMO," *IEEE Wirel. Commun.*, vol. 27, no. 4, pp. 74-80, Aug. 2020.

[3] R. Dai, Y. Liu, Q. Wang, Y. Yu, and X. Guo, "Channel estimation by reduced dimension decomposition for millimeter wave massive MIMO system," *Phys. Commun.*, vol. 44, pp. 101241, Feb. 2021.

[4] S. Lu and Z. Wang, "Training optimization and performance of single cell uplink system with massive-antennas base station," *IEEE Trans. Commun.*, vol. 67, no. 2, pp. 1570-1585, Feb. 2019.

[5] M. Cui and L. Dai, "Channel estimation for extremely large-scale MIMO: Far-field or near-field?" *IEEE Trans. Commun.*, vol. 70, no. 4, pp. 2663-2677, Apr. 2022.

[6] K. Ardah, A. L. F. de Almeida, and M. Haardt, "A gridless CS approach for channel estimation in hybrid massive MIMO systems," in *Proc. IEEE Int. Conf. Acoust., Speech, Signal Process. (ICASSP)*, Brighton, UK, May 2019, pp. 4160-4164.

[7] J. Lee, G.-T. Gil, and Y. H. Lee, "Channel estimation via orthogonal matching pursuit for hybrid MIMO systems in millimeter wave communications," *IEEE Trans. Commun.*, vol. 64, no. 6, pp. 2370-2386, Jun. 2016.

[8] X. Wei and L. Dai, "Channel estimation for extremely large-scale massive MIMO: Far-field, near-field, or hybrid-field?" *IEEE Commun. Lett.*, vol. 26, no. 1, pp. 177-181, Jan. 2022.

[9] X. Wu, X. Yang, S. Ma, B. Zhou and G. Yang, "Hybrid Channel Estimation for UPA-Assisted Millimeter-Wave Massive MIMO IoT Systems," *IEEE Internet Things J.*, vol. 9, no. 4, pp. 2829-2842, Feb. 2022.

[10] K. Shu, X. He, L. Shi and N. Chen, "An OTFS Channel Estimation Scheme Based on Efficient Sparse Bayesian Learning," in *2022 IEEE/CIC International Conference on Communications in China (ICCC)*. IEEE, 2022, pp. 150-155.

[11] Y. Zhang, X. Hu, S. Zhou, and J. Wang, "Channel parameter estimation method in near-field radio environment using SAGE algorithm," *J. Simul.*, vol. 23, no. 9, pp. 1932-1936, Sep. 2011.

[12] C. Liu, J. Sun, W. Zhang and C. -X. Wang, "A New SAGE-Based Channel Estimation Scheme for Millimeter Wave MIMO-OFDM Systems with Hybrid Beamforming Techniques," in *2022 IEEE/CIC International Conference on Communications in China (ICCC)*. IEEE, 2022, pp. 844-849.

[13] W. Ma, C. Qi, and G. Y. Li, "High-resolution channel estimation for frequency-selective mmWave massive MIMO systems," *IEEE Trans. Wirel. Commun.*, vol. 19, no. 5, pp. 3517-3529, May 2020.

[14] X. Zhang, W. Chen, W. Zheng, Z. Xia and Y. Wang, "Localization of near-field sources: A reduced-dimension MUSIC algorithm," *IEEE Commun. Lett.*, vol. 22, no. 7, pp. 1422-1425, Jul. 2018.

[15] J. He, M. N. S. Swamy and M. O. Ahmad, "Efficient Application of MUSIC Algorithm Under the Coexistence of Far-Field and Near-Field Sources," *IEEE Trans. Signal Process.*, vol. 60, no. 4, pp. 2066-2070, Apr. 2012.

[16] W. Zuo, J. Xin, N. Zheng and A. Sano, "Subspace-Based Localization of Far-Field and Near-Field Signals Without Eigendecomposition," *IEEE Trans. Signal Process.*, vol. 66, no. 17, pp. 4461-4476, Sep. 2018.

[17] X. Yin, S. Wang, N. Zhang and B. Ai, "Scatterer Localization Using Large-Scale Antenna Arrays Based on a Spherical Wave-Front Parametric Model," *IEEE Trans. Wirel. Commun.*, vol. 16, no. 10, pp. 6543-6556, Oct. 2017.

[18] L. L. Magoarou, A. L. Calvez, and S. Paquelet, "Massive MIMO channel estimation taking into account spherical waves," in *Proc. IEEE Int. Workshop Signal Process. Adv. Wireless Commun. (SPAWC)*, Cannes, France, Jul. 2019, pp. 1-5.

[19] Z. Huang, B. Xue, W. Wang, F. Dong, and D. Wang, "A Low Complexity Localization Algorithm for Mixed Far-Field and Near-Field Sources," *IEEE Commun. Lett.*, vol. 25, no. 12, pp. 3838-3842, Dec. 2021.